

Dynamic Characterization of MEMS-Tunable Vertical-Cavity SOAs

Garrett D. Cole¹, John E. Bowers², Kimberly L. Turner³, Noel C. MacDonald^{1,3}

1) Materials Department, 2) Electrical and Computer Engineering Department, 3) Mechanical Engineering Department, University of California, Santa Barbara, CA 93106, USA
Phone: +1-805-893-5341, Fax: +1-805-893-8486, Email: gcole@engineering.ucsb.edu

Abstract—We analyze the dynamics of tunable-VC SOAs. At 6 mT the devices exhibit a Q of ~500 and an f_0 of 168.32 kHz. At atmosphere Q is reduced to 1.2 resulting in <10 μ s switching times.

I. INTRODUCTION

Vertical-cavity semiconductor optical amplifiers (VC SOAs) are an attractive alternative to existing amplifier technologies for use in fiber-optic communication systems such as metro-area networks and fiber to the home. In such applications, VC SOAs exhibit a number of advantages including a high coupling efficiency to optical fiber, polarization insensitive gain, decreased power consumption, the potential to fabricate 2-D arrays, and the ability to perform on-wafer testing [1].

For reconfigurable optical networks it is of interest to develop tunable VC SOAs that can cover a wide wavelength range and be precisely adjusted to match the wavelength of the input signal. In Fabry-Pérot SOAs such as VC SOAs, the signal-gain bandwidth is constricted to the linewidth of the resonant cavity mode. With VC SOAs the high mirror reflectivities lead to a narrow gain bandwidth, resulting in spectral filtering of the input signal. In this way VC SOAs may be utilized as amplifying filters. Incorporating tunability allows for the creation of wavelength agile filters with gain.

A promising approach to achieve rapid, low power, and wide wavelength tuning is through the use of an integrated microelectromechanical (MEMS) actuator [2], [3]. Here, mechanical alteration of the effective cavity length gives rise to tuning ranges greater than those that can be achieved by refractive index modulation [4]. Recently, we demonstrated the first widely tunable VC SOA, utilizing an integrated AlGaAs-based electrostatic actuator for wavelength tuning [2]. We present here a detailed dynamic analysis of our MEMS-tunable VC SOA (MT-VC SOA).

II. DEVICE DESIGN AND FABRICATION

The MT-VC SOA utilizes a micromachined electrostatic actuator to vary the position of a suspended distributed Bragg reflector (DBR). The freestanding portion of the actuator consists of a central mass, made up of a 5-period GaAs/Al_{0.98}Ga_{0.02}As DBR pillar, suspended by four composite SiN_x/GaAs springs, as seen in Fig. 1(a). In these devices a thin layer of tensile-stressed (260 MPa) SiN_x is deposited on top of the GaAs membrane prior to release to ensure the flatness of the free-standing structure. From the top down the actuator material structure consists of a 350-nm thick GaAs membrane layer, a 1950-nm Al_{0.98}Ga_{0.02}As sacrificial etch layer (selectively removed with a dilute HCl solution, resulting in an air gap of approximately the same thickness), and a 115-nm GaAs contact layer, directly above the multiquantum well (MQW) active region. As shown in Fig. 1(b), the GaAs layers straddling the air gap are doped n⁺, while the sacrificial AlGaAs layer is comprised of 200 nm of p⁺ Al_{0.98}Ga_{0.02}As,

followed by 1750 nm of intrinsic Al_{0.98}Ga_{0.02}As. A reverse bias across this n⁺/p⁺/i/n⁺ diode results in a Coulomb force on the freely suspended membrane. Upon actuation, the decrease in air-gap thickness leads to a reduction in the effective cavity length and a blue shift in the wavelength of peak gain. A detailed description of the optical design as well as the fabrication procedure can be found in [3].

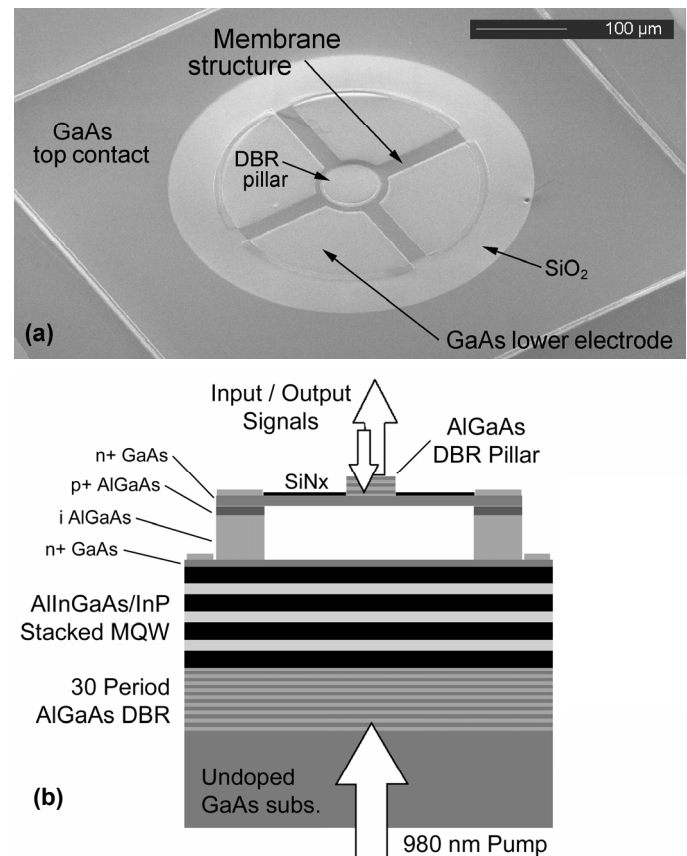


Fig. 1. (a) Scanning electron micrograph of the electrostatic actuator. (b) Cross-sectional schematic of the MT-VC SOA material structure.

III. DYNAMIC TESTING AND RESULTS

The dynamic response of the actuator was tested both in vacuum (6 mT) and at atmosphere using a multidimensional MEMS-motion characterization system [5]. In this test setup, a square-root sinusoidal drive signal $V = V_A \sqrt{1 + \cos(\omega t)}$ was supplied by a function generator. Because the force of the electrostatic actuator is proportional to V^2 , the use of the root-sinusoid results in a forcing function at the desired frequency, plus an additional DC offset. Out of plane motion was detected with a laser Doppler vibrometer and the resulting velocity and displacement signals were captured and analyzed using a vector signal analyzer and oscilloscope. Fig. 2 shows a typical response of the actuator for small excitation amplitude

(2 V) in vacuum (6 mT). Here the actuator exhibits a simple harmonic response with a resonant frequency f_0 of 168.32 kHz and a mechanical quality factor (Q) of 491 determined from the width of the resonance peak. The small amplitude response in vacuum allows for the extraction of the intrinsic damping of the actuator as well as the natural frequency ω_0 .

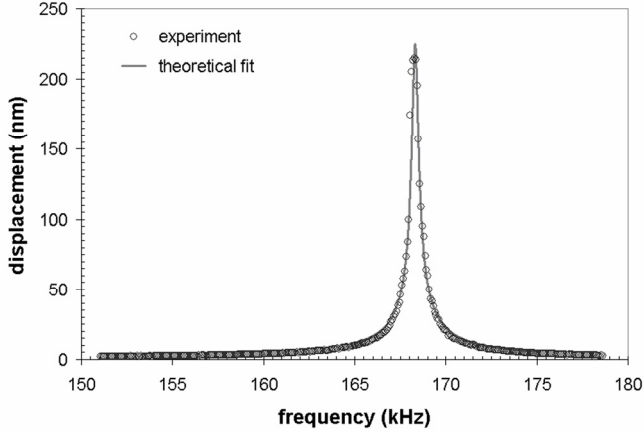


Fig. 2. Simple harmonic response of the MT-VCSOA at a pressure of 6 mT and driving amplitude of 2 V.

With increasing drive voltage the response becomes asymmetric and beyond a critical amplitude develops a hysteretic response (Fig. 3) typical of a hardening spring Duffing oscillator, arising from the nonlinear restoring force of the doubly-clamped springs. By sweeping up and down in the applied frequency, the bistable region of the response curve may be determined. With increasing displacement C , the nonlinear resonance ω_{nl} shifts to higher frequency with [6]:

$$\omega_{nl} = \sqrt{\omega_0^2 + \frac{3}{4}\mu C^2} \quad (1)$$

where μ is the coefficient of nonlinearity and is simply the cubic spring constant k_3 divided by the effective mass of the actuator m_{eff} . Recording the frequency of the nonlinear resonance peak for different amplitudes and plotting ω_{nl}^2 versus C^2 results in a linear function, with a y-intercept of ω_0^2 and slope of $3/4\mu$ as demonstrated in the upper left of Fig. 3. This procedure allows for the determination of k_3 without the need for fitting of the individual response curves.

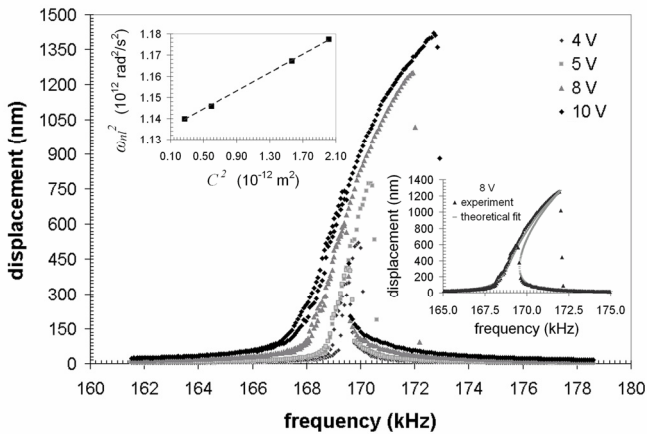


Fig. 3. Duffing response of the electrostatic actuator at 6 mT.

For the device analyzed in Fig. 3 we find that the coefficient of nonlinearity $\mu = 3.35 \times 10^{22} \text{ m}^{-2} \text{ s}^{-2}$ ($k_3 = 1.28 \text{ } \mu\text{N}/\mu\text{m}^3$). Combined with the damping coefficient extracted from the

harmonic fit it is possible to generate theoretical curves for the nonlinear response of the actuator, as in Fig. 3.

Operation of the MT-VCSOA in vacuum allows for the accurate determination of the intrinsic damping, natural frequency, and nonlinear characteristics of the actuator. However, the lack of significant viscous damping in vacuum leads to excessive ringing and long settling times. For the intended application it is desirable to increase the damping in order to minimize the response time, assuming the device remains underdamped. Because of the large ratio of lateral dimensions to air-gap thickness, squeeze film damping is significant at increased pressure. In comparison with testing in vacuum, at atmosphere the Q is reduced considerably to 1.2, as seen below in Fig. 4. This device is slightly underdamped with a damped resonant frequency f_d of roughly 150 kHz. Given these properties we find that at atmosphere the approximate settling time, defined as the time to reach $\pm 5\%$ of the final displacement value, is $5.7 \text{ } \mu\text{s}$. Thus, the MT-VCSOA is capable of achieving a 10-nm wavelength shift (displacement of roughly 75 nm [3]) in less than $10 \text{ } \mu\text{s}$.

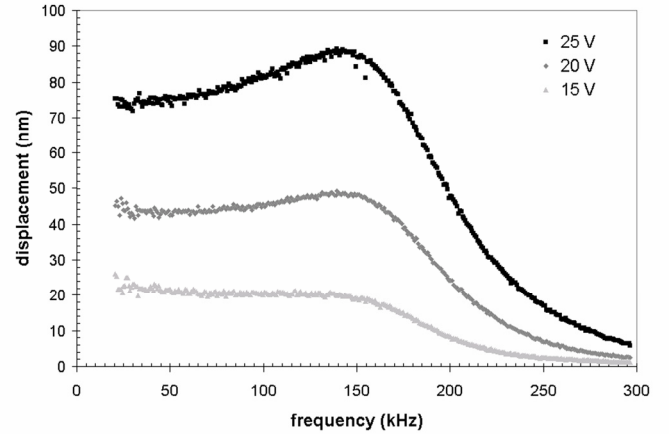


Fig. 4. Dynamic response of the MT-VCSOA at atmosphere. For each curve the measured quality factor is 1.2

IV. SUMMARY

The dynamic response of our MT-VCSOA has been characterized in vacuum and at atmosphere using a laser Doppler vibrometer. At 6 mT and for small displacements the actuator presented here exhibits a simple harmonic response with a Q of 491, while for large displacements the device exhibits a hardening spring Duffing response with $k_3 = 1.28 \text{ } \mu\text{N}/\mu\text{m}^3$. At atmosphere the actuator exhibits significant squeeze film damping, reducing the Q to 1.2. The frequency response in air is underdamped and is found to exhibit settling times of less than $10 \text{ } \mu\text{s}$.

V. REFERENCES

- [1] E. S. Björilin, T. Kimura, J. E. Bowers, *IEEE J. Select. Topics Quantum Electron.*, vol. 9, pp. 1374-1385, Sep./Oct. 2003.
- [2] Q. Chen, G. D. Cole, E. S. Björilin, T. Kimura, S. Wu, C. S. Wang, N. C. MacDonald, J. E. Bowers, *IEEE Photon. Technol. Lett.*, vol. 16, pp. 1438-1440, June 2004.
- [3] G. D. Cole, E. S. Björilin, Q. Chen, C.-Y. Chan, S. Wu, C. S. Wang, N. C. MacDonald, J. E. Bowers, *IEEE J. Quantum Electron.*, vol. 41, pp. 390-407, March 2005.
- [4] T. Kimura, E. S. Björilin, J. Piprek, J. E. Bowers, *IEEE Photon. Technol. Lett.*, vol. 15, pp. 1501-1503, Nov. 2003.
- [5] K. Turner, P. Hartwell, and N. Macdonald, in *Digest of Technical Papers Transducers '99*, Sendai, Japan, 1999.
- [6] P. Hagedorn, *Non-Linear Oscillations*, New York, NY: Oxford University Press, 1988, pp. 1-59.